



LAWRENCE
LIVERMORE
NATIONAL
LABORATORY

ELM-Induced Plasma Wall Interactions in DIII-D

D. L. Rudakov, J. A. Boedo, J. H. Yu, N. H. Brooks, M. E. Fenstermacher, M. Groth, E. M. Hollmann, C. J. Lasnier, A. G. McLean, R. A. Moyer, P. C. Stangeby, G. R. Tynan, W. R. Wampler, J. G. Watkins, W. P. West, C. P. C. Wong, L. Zeng, R. J. Bastasz, D. Buchenauer, J. Whaley

May 15, 2008

18th International Conference on Plasma Surface Interactions
Toledo, Spain
May 26, 2008 through May 30, 2008

Disclaimer

This document was prepared as an account of work sponsored by an agency of the United States government. Neither the United States government nor Lawrence Livermore National Security, LLC, nor any of their employees makes any warranty, expressed or implied, or assumes any legal liability or responsibility for the accuracy, completeness, or usefulness of any information, apparatus, product, or process disclosed, or represents that its use would not infringe privately owned rights. Reference herein to any specific commercial product, process, or service by trade name, trademark, manufacturer, or otherwise does not necessarily constitute or imply its endorsement, recommendation, or favoring by the United States government or Lawrence Livermore National Security, LLC. The views and opinions of authors expressed herein do not necessarily state or reflect those of the United States government or Lawrence Livermore National Security, LLC, and shall not be used for advertising or product endorsement purposes.

ELM-Induced Plasma Wall Interactions in DIII-D

D.L. Rudakov^{a*}, J.A. Boedo^a, J.H. Yu^a, N.H. Brooks^b, M.E. Fenstermacher^c, M. Groth^c,
 E.M. Hollmann^a, C.J. Lasnier^c, A.G. McLean^d, R.A. Moyer^a, P.C. Stangeby^d, G.R. Tynan^a,
 W.R. Wampler^e, J.G. Watkins^e, W.P. West^b, C.P.C. Wong^b, L. Zeng^f, R.J. Bastasz^g, D.
 Buchenauer^g, J. Whaley^g

^a*University of California, San Diego, La Jolla, California 92093-0417, USA*

^b*General Atomics, San Diego, California 92186-5608, USA*

^c*Lawrence Livermore National Laboratory, Livermore, California 94550, USA*

^d*University of Toronto Institute for Aerospace Studies, Toronto, M3H 5T6, Canada*

^e*Sandia National Laboratories, Albuquerque, New Mexico 87185-1129, USA*

^f*University of California, Los Angeles, California, USA*

^g*Sandia National Laboratories, Livermore, California 94550, USA*

Abstract

Intense transient fluxes of particles and heat to the main chamber components induced by edge localized modes (ELMs) are of serious concern for ITER. In DIII-D, plasma interaction with the outboard chamber wall is studied using Langmuir probes and optical diagnostics including a fast framing camera. Camera data shows that ELMs feature helical filamentary structures localized at the low field side of the plasma and aligned with the local magnetic field. During the nonlinear phase of an ELM, multiple filaments are ejected from the plasma edge and propagate towards the outboard wall with velocities of 0.5-0.7 km/s. When reaching the wall, filaments result in “hot spots” — regions of local intense plasma-material interaction (PMI) where the peak incident particle and heat fluxes are up to 2 orders of magnitude higher than those between ELMs. This interaction pattern has a complicated geometry and is neither toroidally nor poloidally symmetric. In low density/collisionality H-mode discharges, PMI at

the outboard wall is almost entirely due to ELMs. In high density/collisionality discharges, contributions of ELMs and inter-ELM periods to PMI at the wall are comparable. A Midplane Material Evaluation Station (MiMES) has been recently installed in order to conduct *in situ* measurements of erosion/redeposition at the outboard chamber wall, including those caused by ELMs.

JNM keywords:

PSI-18 keywords: DIII-D,

PACS:

**Corresponding author address: 9500 Gilman Dr, Mail code 0417, La Jolla, CA 92093-0417*

**Corresponding author e-mail: rudakov@fusion.gat.com*

Presenting author address: as above

Presenting author e-mail: as above

I. Introduction

Limiting plasma-material interactions (PMI) to acceptable levels presents one of the toughest challenges for the next-step fusion devices such as the International Thermonuclear Experimental Reactor (ITER) [1]. The plasma facing components (PFCs) in ITER have to withstand incident fluxes of particles and energy orders of magnitude higher in magnitude and duration than those encountered in the present day tokamaks [1]. Though most of the energy and particles crossing the last closed flux surface (LCFS) into the scrape-off layer (SOL) are expected to sink into the divertor where the PMI will be most strong [2], plasma contact with the main chamber components will also be non-negligible. Of particular concern are the impulsive loads due to transient events such as disruptions and edge-localized modes (ELMs) [1,3-11]. Studies at contemporary tokamaks have shown that ELMs can drive significant part of the total particle and energy exhaust to the main chamber PFCs [6-11]. Moreover, it has been shown that ELMs in the SOL have a filamentary structure [4,6,7,9-11], and individual filaments reaching the main chamber wall can cause localized “hot spots” where the PMI is particularly intense [9,11]. If this happens in ITER, it may cause local melting of the beryllium PFCs, leading to enhanced erosion and increased dust production. Sufficiently large gaps between the wall and the separatrix and/or additional protection limiters may be needed to avoid this problem.

In this article we report continuation of studies of the plasma interaction with the main chamber wall in the DIII-D tokamak with the emphasis on ELM-caused PMI. Results from new diagnostics that recently became available and an extended analysis of the pre-existing data are presented.

II. Structure of the DIII-D outboard SOL and diagnostic arrangement

DIII-D [12] is a tokamak with major and minor radii of 1.67 m and 0.67 m, and all-carbon (graphite) PFCs. Figure 1 shows a poloidal cross-section of DIII-D tokamak with LCFS and a few SOL magnetic flux surfaces for a lower single-null (LSN) discharge. There are three distinct regions in the low field side (LFS) SOL [9]. “Divertor SOL” (DSOL) is the region where the magnetic field lines connect from the outboard to the inboard side of the torus. “Limiter SOL” (LSOL) is the region where both sides of the magnetic field lines terminate on the divertor baffles. The radial width of LSOL depends on the magnetic topology; in configurations with a large upper gap (UG) and/or small outer wall gap (OWG) LSOL may totally vanish. Further outwards from the LSOL is the “Outer Wall Shadow” (OWS) region, where the magnetic field lines terminate at the outer wall near the midplane. There are three bumper limiters (BLs, see Fig. 2(a)) on the outer wall separated toroidally by approximately 120 degrees and protruding by ~ 2 cm inwards from the wall tile radius.

Previous studies of the plasma interaction with LFS chamber wall in DIII-D relied almost exclusively on the mid-plane reciprocating probe array (RCP) [13] and a fast profile reflectometer [14]. A few new diagnostics have been recently commissioned. A fast framing CMOS camera (Phantom 7.1) has a tangential view of the outboard chamber wall with a spatial resolution of about 5 mm [11]. The camera has framing rate of up to 26000 frames/s at 256×256 pixel resolution. A filterscope (telescope with spectral line filter coupled to a photomultiplier) [15] has a view of a mid-plane portion of a bumper limiter and another one has a view of the wall tiles nearby [Fig. 2(a)]. In addition, a capability to install material samples at the outer shield of the RCP (so-called Mid-plane Material Evaluation Station or MiMES) [16] has been recently implemented. This allows *in situ* measurements of net erosion/deposition at the LFS chamber wall. Samples can be exchanged through an airlock. A

photograph of MiMES inside the airlock chamber is shown in Fig. 2(b). Locations of depth-marked graphite button samples on the plasma-facing side of MiMES are marked by arrows.

III. Experimental results

ELM propagation through the LFS SOL and interaction with the outboard wall were studied in LSN H-mode discharges with the following parameters: toroidal magnetic field, $B_T = 1.7 - 2.1$ T, plasma current, $I_p = 1 - 1.4$ MA, neutral beam heating power, $P_{\text{NBI}} = 1.5 - 7$ MW, line-average plasma density, $\bar{n}_e = 0.5 - 1.2 \times 10^{20} \text{ m}^{-3}$, density normalized to Greenwald limit, $f_{\text{GW}} \equiv n_e/n_{\text{GW}} = 0.35 - 1$.

Fast camera data shows that ELMs in the LFS edge and SOL feature helical filamentary structures aligned with the local magnetic field. Figure 3(a,b) shows ELM filaments imaged in CIII light in low ((a), $f_{\text{GW}} = 0.35$) and moderate ((b), $f_{\text{GW}} = 0.7$) density discharges. Toroidal mode number, n , increases with discharge density from 10 – 20 in the low density case at to over 30 at higher density [11]. During the nonlinear phase of an ELM, multiple filaments are ejected from the plasma edge and propagate radially outwards through the SOL. These observations are consistent with the previous probe measurements showing that ELMs in the SOL have fine structure with multiple bursts of ion saturation current measured during each ELM [3,5-7,9]. Radial propagation velocity of the filaments estimated from the camera data at 500 ± 400 m/s is consistent with the ExB velocity of ~ 700 m/s inferred from the probe data [6,7] and propagation velocity of the ELM density pulse of ~ 500 m/s estimated from the reflectometer data [3]. Upon reaching the wall, the filaments cause PMI that is clearly observed in D_α emission [Fig 3(c,d)] due to release of neutrals from the wall tiles. Localized areas of intense PMI (“hot spots”) are observed in both the low and moderate density cases, however, in the lower density case their relative brightness is much larger. This is consistent with an earlier conclusion made from the probe data that the relative contribution of the ELMs to the (parallel) particle flux arriving at the outboard wall decreases from 80-90% at $f_{\text{GW}} = 0.4$ -

0.5 to about 30% at $f_{GW} \sim 1$ [9]. Figure 4 shows results of similar analysis applied to the parallel heat flux, $q_{\parallel} = 7kT_e j_{si} / e$, where T_e is the electron temperature and j_{si} is the ion saturation current density measured by the probe near the outer edge of LSOL (which should be representative of the wall conditions [9]). Similar trend is observed, but the relative contribution of ELMs to the net local heat flux is somewhat higher compared to the particle flux. This is not surprising, considering that both n_e and T_e inside ELM filaments are above the background values [6,7,9].

While propagating through the SOL, ELM filaments are depleted of particles and energy by parallel losses, and may partially or fully decay before reaching the wall [6,7,9]. This is illustrated in Figure 5 showing radial profile of the peak ion saturation current, I_{sat} , within ELM filaments (squares) measured by RCP in far SOL of a high density ($f_{GW} \sim 1$) discharge. The discharge had a large upper gap (9.3 cm) and no LSOL. Within the radial distance of ~ 4 cm shown in the plot, filament amplitude decays by almost two orders of magnitude. Throughout the region shown it stays about 10 times above the inter-ELM background (diamonds). Later in the discharge the outer wall gap was transiently reduced by 3 cm from ~ 9.3 to ~ 6.3 cm [Fig. 6(a)]. This resulted in increase in both filament amplitude and background density in DSOL and throughout most of the OWS region [Fig. 5(b)]. BL and wall filterscopes evidenced increased PMI at the LFS wall manifesting itself by an increase in D_{α} emission during the discharge phase with the decreased OWG [Fig. 6(b), BL filtescope signal shown]. In subsequent discharges the wall gap was transiently increased from 9.3 to 12.3 cm [Fig. 6(d)]. Corresponding decrease of the D_{α} emission was observed by the filterscopes [Fig. 6(e)]. Thus a moderate change of the OWG has a significant effect at the level of plasma interaction with the LFS wall.

Graphite button samples installed on the plasma-facing side of MiMES [Fig. 2(b)] were exposed in 7 high density H-mode discharges similar to those illustrated in figures 5 and 6.

During the exposure the samples were in OWS (~ 0.5 cm outside of the DSOL border) for a total of ~ 16 seconds and in DSOL (~ 1.5 cm inside of OWS border) for ~ 12 seconds. The samples have implanted Si depth marker that allows measuring net erosion/deposition by Ion Beam Analysis (in progress at Sandia National Laboratories Albuquerque). RCP was fixed during the exposure so that the tips measuring I_{sat} were about 5mm inwards of the sample location, as shown in Fig. 2(b). During OWG scans ion saturation current measured by the probe behaved similarly to D_α emission measured by BL and wall filterscopes [Fig. 6 (c,f)]. Note that the probe position was 2 cm further inwards during the inward OWG scan in Fig. 6(d-f) compared to the outward OWG scan in Fig. 6(a-c).

IV. Summary and conclusion

We presented experimental evidence showing that ELMs cause significant plasma interaction with the main chamber wall in DIII-D. Relative contribution of ELMs to PMI with the LFS chamber wall decreases with increasing discharge density, which in DIII-D is coupled to increasing pedestal collisionality. Since ITER will have high normalized density and low collisionality, it's not quite clear how large will the relative importance of ELMs for the main chamber PMI be. Even at high density close to the Greenwald limit, ELM filaments may reach the LFS wall and cause erosion of the wall tiles. A moderate increase of the gap between LCFS and the wall may appreciably decrease PMI intensity. Therefore, if ELM interaction with the main chamber wall turns out a problem in ITER, provision for an increased wall gap may be extremely helpful.

Acknowledgment

Work supported by the U.S. Department of Energy under DE-FG02-07ER54917, DE-FC02-04ER54698, DE-AC52-07NA27344 with LLNL, and DE-AC02-76CH03073, and DE-AC04-94AL85000.

References

- [1] G. Federici, *et al.*, Nucl. Fusion **41** (2001) 1967.
- [2] P.C. Stangeby, *The Plasma Boundary of Magnetic Fusion Devices*, IoP Publishing, 2000.
- [3] M.E. Fenstermacher, *et al.*, Plasma Phys. Control. Fusion **45** (2003) 1597.
- [4] A. Kirk, *et al.*, Phys. Rev Lett. **92** (2004) 245002.
- [5] D.L. Rudakov, *et al.*, J. Nucl. Mater. **337–339** (2005) 717.
- [6] J.A. Boedo, *et al.*, J. Nucl. Mater. **337–339** (2005) 771.
- [7] J.A. Boedo, *et al.*, Phys. Plasmas **12** (2005) 072516.
- [8] D.G. Whyte, *et al.*, Plasma Phys. Control. Fusion **47** (2005) 1579.
- [9] D.L. Rudakov, *et al.*, Nucl. Fusion **45** (2005) 1589.
- [10] B. Lipschultz, *et al.*, Nucl. Fusion **47** (2007) 1189.
- [11] J. H. Yu, *et al.*, Phys. Plasmas **15** (2008) 032504.
- [12] J. L. Luxon, Nucl. Fusion **42**, 614 (2002).
- [13] J.G. Watkins, *et al.*, Rev. Sci. Instrum. **63** (1992) 4728.
- [14] L. Zeng, *et al.*, Rev. Sci. Instrum. **74** (2003) 1530.
- [15] R. J. Colchin, *et al.*, Rev. Sci. Instrum. **74** (2003) 2068.
- [16] C.P.C. Wong, *et al.*, J. Nucl. Mater. **363–365** (2007) 276.

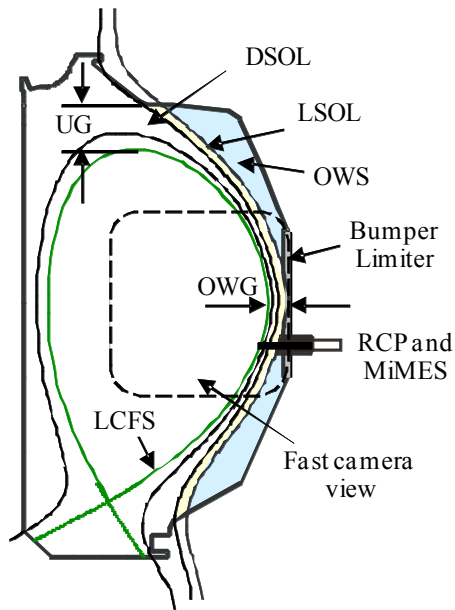


Fig. 1. Diagnostic arrangement and structure of the DIII-D SOL in a LSN magnetic configuration.

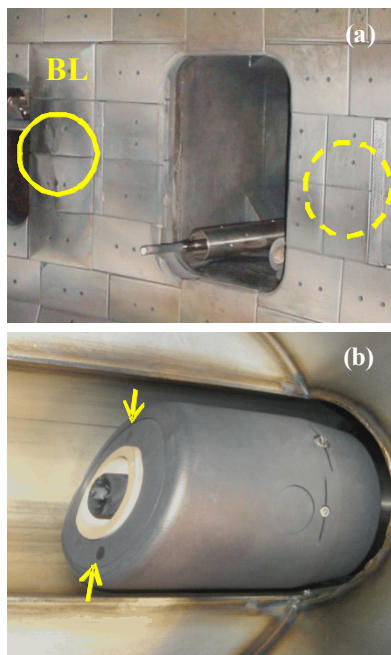


Fig. 2. Photographs of (a) portion of LFS chamber wall showing a bumper limiter, views of the bumper limiter (solid circle) and wall (dashed circle) filterscopes, and mid-plane RCP with the outer shield removed; (b) RCP with MiMES inside the airlock chamber.

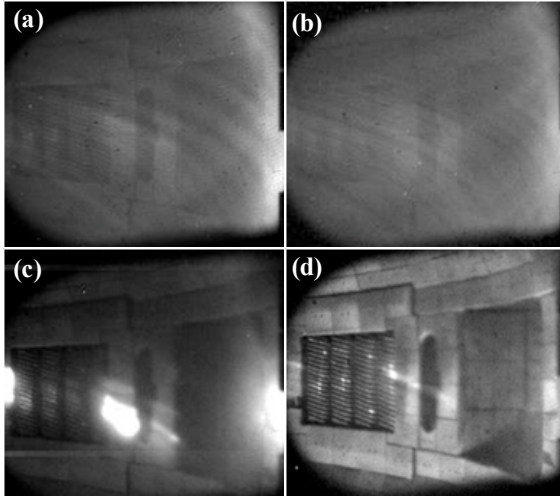


Fig. 3. Fast camera images of ELM filaments in CIII light near the separatrix (a,b) and in D_α light interacting with the outboard wall (c,d) in low (a,c) and moderate (b,d) density discharges.

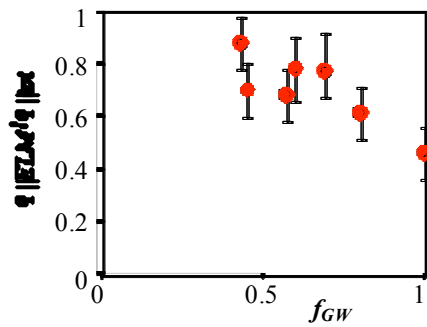


Fig. 4. Relative contribution of ELMs to the local parallel heat flux at the outer edge of LSOL as a function of the normalized discharge density

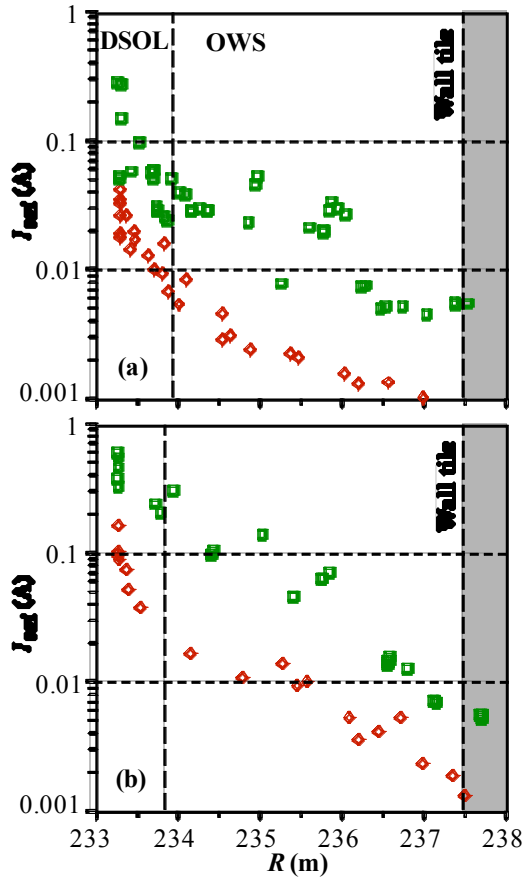


Fig. 5. Radial profiles of the peak ion saturation current within ELM filaments (squares) and between-ELM background (diamonds) in far SOL of a high density ($f_{GW} \sim 1$) LSN discharge with OWG of 9.5 cm (a) and 6.5 cm (b).

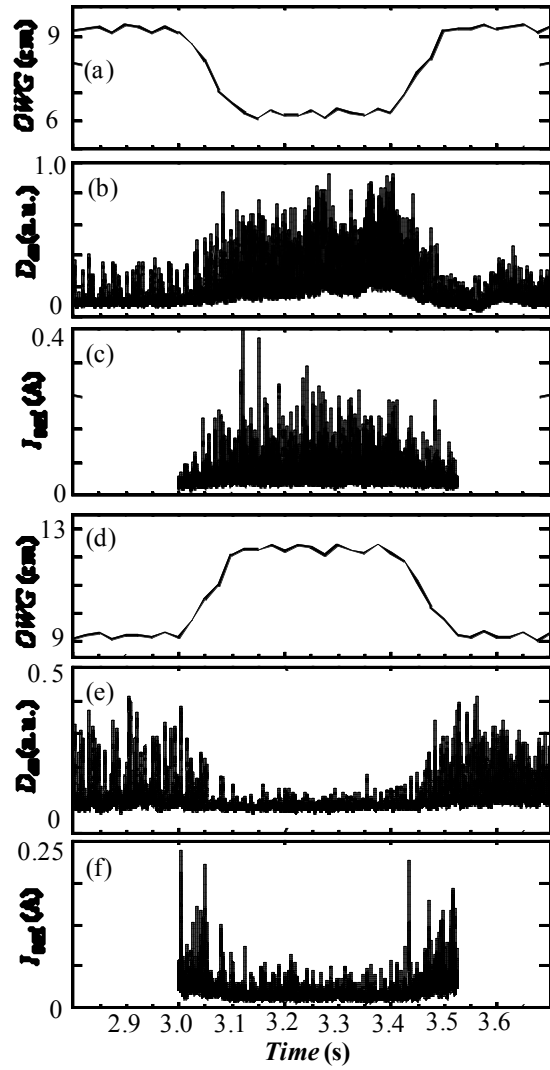


Fig. 6. Changes in outer wall PMI with decreased (a-c) and increased (d-f) outer wall gap. Shown are D_α emission measured by BL filterscope (b,e) and ion saturation current to a probe fixed at the LSOL/OWS boundary (c) and about 2 cm into LSOL (d).